JOURNAL OF MATERIALS SCIENCE 24 (1989) 2221–2230

Stable crack growth, instability, fatigue and fracture of a 50/50 blend of poly(2,6-dimethyl-1,4-phenylene oxide) and polystyrene

MICHAEL T. TAKEMORI, THOMAS A. MORELLI*, JAMES McGUIRE‡
Polymer Physics and Engineering Laboratory, GE Corporate Research and Development Center, Schenectady, New York, 12301 USA

The fracture behaviour of a 50/50 blend of poly(2,6-dimethyl-1,4-phenylene oxide)/polystyrene has been studied. The crack propagation behaviour is strongly influenced by the temperature, crack driving force and the nature of the crack tip craze zone. A fracture map outlining the regions of stable crack growth as a function of temperature, crack velocity and crack driving force has been determined. At high temperatures and low crack growth velocities, stable crack propagation proceeds through a single-craze crack tip damage zone, while at lower temperatures and high crack velocities, a multiple-craze crack tip zone is observed. Corresponding behaviour can be observed under fatigue loading conditions. An instability leading to very high-speed fracture occurs at a critical crack velocity, thus limiting the stable crack propagation regime to lower velocities. The various reported measures of fracture toughness, such as those based on crack initiation, peak load and the onset of crack instability, are discussed.

1. Introduction

The stable crack growth behaviour in many polymers can be described by a fracture map, which gives the relationship between crack velocity and crack driving force [1–19]. Such fracture maps are schematically illustrated in Fig. 1. The crack driving force is usually given in terms of the stress intensity factor (K) or a strain energy release rate (G) when linear elastic conditions exist. During stable crack growth, the crack velocity increases with increasing crack driving force in a unique relationship. The initial period of crack growth, however, depends strongly on crack initiation processes and the crack preparation conditions. At a critical crack velocity, typically between 1 and 10 cm sec^{-1}, cracks become unstable and a sudden transition to very rapid fracture, with speeds in excess of 100 m sec^{-1}, can be observed. Fracture maps have been identified for PMMA [1–12], PC [13, 14], PES [15], HDPE [16] and PVC [17].

When cracks propagate by advancing through a leading crack tip craze (or crazes), the crack growth resistance is primarily determined by the strength and number of these crack tip crazes. Recent studies by Schirrer and Goett [20] have shown that many amorphous polymers exhibit a critical temperature above which a single craze grows ahead of the propagating crack and below which multiple crazes grow. This transition to a single craze at high temperatures is accompanied by a reduction in fracture toughness.

In this paper, the results of a study on the fracture behaviour of a compatible 50/50 blend of poly(2,6-dimethyl-1,4-phenylene oxide)/polystyrene (PPO/PS) will be presented. Three issues will be discussed. (1) A fracture map for this blend will be presented, showing the stable crack growth dependence on temperature and crack driving force and the onset of crack instability. For this blend, the crack tip plastic zone (crazing) was confined to a reasonably small volume of material near the crack tip such that the macroscopic load conditions were linear elastic (until crack growth commenced). Therefore, the mode I stress intensity factor, K_I, was used to characterize the crack driving force (all results refer to mode I, hence the subscript I will be omitted in this paper). (2) The transition from a multiple-craze crack tip zone to a single-craze crack tip zone was examined. Corresponding behaviour under fatigue loading was also studied. (3) The various measures of fracture toughness are discussed in the light of the strong temperature and driving force dependence of crack propagation and the fracture instability at high speeds.

2. Experimental methods

A 50/50 miscible blend of PPO/PS was injection

*Present address: GE Plastics, Pittsfield, Massachusetts, USA.
‡Present address: ARCO, Newtown Square, Pennsylvania, USA.

0022–2461/89 $03.00 + .12

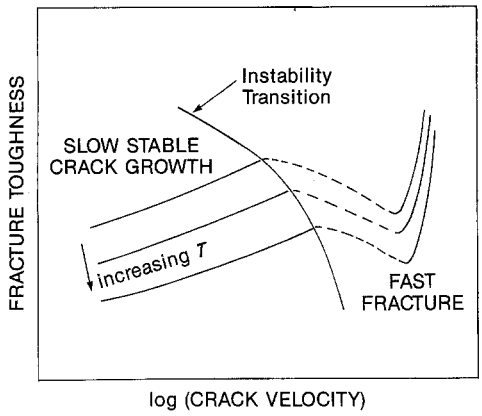

Figure 1 Schematic fracture map for amorphous polymers. The ordinate represents some measure of crack driving force or fracture toughness, e.g. K or G. To the right of the instability transition, the dashed lines represent a "forbidden" unstable zone where crack velocity increases with decreasing driving force. Crack propagation is not observed in this regime. In the fast fracture zone, typical crack speeds are of the order of 100 m sec^{-1}.

moulded into 0.64 cm thick plaques from which compact tension samples were machined (Fig. 2). The samples were prepared according to ASTM E-399 [21] with W = 5.33 cm and B = 0.64 cm. The only deviation from the standard was that the diameter of the loading holes was $0.194W$ instead of the recommended $0.25W$.

Starter cracks were prepared by sinusoidal fatigue loading under load control at 100° C. The 100° C temperature was chosen to ensure a single-craze plastic zone at the crack tip (to be further elucidated). Great care was taken not to exceed 1 h at this elevated temperature because evidence had indicated that long exposures could lead to thermal embrittlement. The fatigue crack was grown with a minimum to maximum load ratio of 0.1 at 20 Hz. A final maximum K value of 1.2 MPa m$^{1/2}$ was selected.

Both the fatigue precracking and the subsequent crack growth testing were performed on an Instron Model 1350 servohydraulic testing machine. Temperatures were controlled to 0.5° C and the samples were maintained at the test temperature for 1 h prior to testing to ensure thermal equilibrium. Crack growth was monitored and recorded with a video camera, which was synchronized with a Nicolet digital storage oscilloscope and a video frame counter. Crack lengths were measured by direct visual observations or with an X–Y video position analyser from the video recordings, whichever was more convenient. A Hewlett-Packard 9816 computer was used to analyse the data.

Stress intensity factors were calculated from the following expression [21]

$$K = \frac{PY(x)}{BW} \tag{1}$$

where $x = a/W$, a is the crack length, P is the applied load and B and W are sample dimensions given in Fig. 2. Y is a geometric factor given by

$$Y = \frac{(2 + x)(0.886 + 4.64x - 13.32x^2 + 14.72x^3 - 5.64x^4)}{(1 - x)^{3/2}} \tag{2}$$

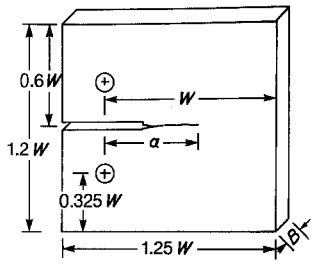

Figure 2 The compact tension samples, with W = 5.33 cm and B = 0.64 cm, used in this study.

3. Fracture concepts, crack velocity, instability

The stress intensity factor, K, and the strain energy release rate, G, have both been used extensively to characterize the crack driving force during the fracture process. K is a parameter describing the stress state, σ, at a point (r, θ, ϕ) near a crack tip

$$\sigma(r, \theta, \phi) = \frac{Kf(\theta, \phi)}{(2\pi r)^{1/2}} \tag{3}$$

while G is given by

$$G = \frac{P^2}{2B}\frac{dC}{da} \tag{4}$$

where C is the sample compliance and P is the load. When any inelastic or plastic effects are limited to a small volume of material near the crack tip such that the macroscopic load conditions are linear elastic, G and K can be related by

$$G = \frac{MK^2}{E} \tag{5}$$

where $M = 1$ for plane stress conditions and $M = 1 - \nu^2$ for plane strain conditions (ν is Poisson's ratio).

Under linear elastic conditions and for stable crack growth, the crack velocity ($v = da/dt$) can be related to the external displacement rate (dD/dt) by substituting for the compliance ($C = D/P$, D = displacement) in Equation 4

$$G = \frac{P^2}{2B}\left(\frac{1}{P}\frac{dD}{da} - \frac{D}{P^2}\frac{dP}{da}\right) \tag{6}$$

For crack velocity: rearranging and dividing by dt gives

$$\frac{da}{dt} = \left[\frac{P}{2BG + D(dP/da)}\right]\frac{dD}{dt} \tag{7}$$

For crack instability: when stable crack growth gives way to unstable fast fracture, the crack instability can be expressed by

$$\frac{dD}{da} = 0 \tag{8}$$

i.e. when an infinitesimal increase in load line displacement (dD) leads to a very large amount of crack growth (da).

Following the work by Gurney and Hunt [22], the onset of fracture instability can be further examined by rewriting Equation 4 in terms of D and C

$$G = \frac{D^2}{2BC^2}\frac{dC}{da} \quad (9)$$

Taking the logarithmic differential with respect to crack length yields

$$\frac{1}{G}\frac{dG}{da} + \frac{1}{C}\frac{dC}{da} - \frac{d^2C}{da^2}\Big/\frac{dC}{da} = 0 \quad (10)$$

Thus, when crack instability occurs, Equation 8 holds and an instability criterion can be obtained from Equation 10

$$\frac{1}{G}\frac{dG}{da} + \frac{1}{C}\frac{dC}{da} - \frac{2}{D}\frac{dD}{da} - \frac{d^2C}{da^2}\Big/\frac{dC}{da} = 0 \quad (11)$$

An alternate instability criterion has been described by Clausing [23] using the general form for K

$$K = \frac{P}{BW^{1/2}}x^{1/2}Y(x) \quad (12)$$

Substituting this into Equation 5 leads to

$$G = \frac{MY^2D^2x}{EB^2WC^2} \quad (13)$$

The logarithmic differentials yield

$$\frac{dG}{G} = Q\,dx + 2\frac{dD}{D} \quad (14)$$

where

$$Q = \frac{2}{Y}\frac{dY}{dx} + \frac{1}{x} - \frac{2}{C}\frac{dC}{dx} \quad (15)$$

Solving for dD/dx gives:

$$\frac{dD}{dx} = \frac{D}{2G}\left[\frac{dG}{dx} - QG\right] \quad (16)$$

Again, instability occurs when dD/dx vanishes (Equation 8), or

$$\frac{1}{G}\frac{dG}{dx} - Q = 0 \quad (17)$$

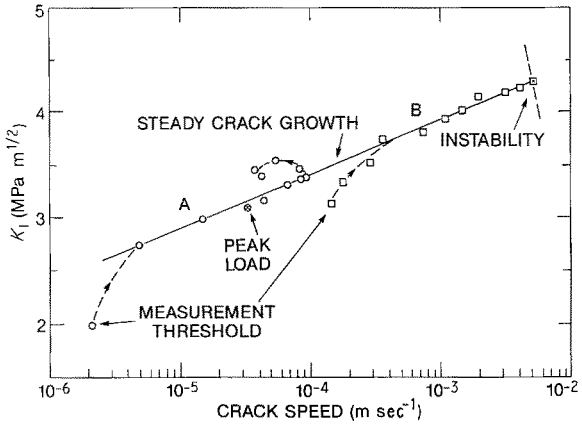

Figure 3 Crack growth data for two samples tested at two different rates: (○) 2.5×10^{-6}, (□) 5.1×10^{-4} m sec^{-1}. Each set of data shows an initiation "tail" at low crack speeds and steady crack growth behaviour.

Equations 11 and 17 represent two crack instability conditions which will be examined in this paper.

4. Results and discussion

4.1. Crack growth (K–crack velocity) fracture map

Fig. 3 shows two typical results at 27° C for constant displacement rate tests of PPO/PS. Each curve represents K–log v data from a single compact tension sample, one showing completely stable crack growth (A) and the other, stable crack growth followed by unstable fast fracture (B). For each sample, data spanned two orders of magnitude in crack velocity. For each case, a crack growth initiation "tail" was observed at low K values, with a rapid rise in K with increasing crack velocity until a relatively linear crack growth curve was attained.

The crack growth initiation tail occurred at different crack velocities for the two samples shown in the figure. When the testing rate was increased by two orders of magnitude (from A to B in Fig. 3), the minimum velocities that were measured also increased by two orders of magnitude. This correlation between the testing rates and the minimum measurable crack velocities is due to the limiting resolution of the measuring system. In attempting to attain the "sharpest" crack possible, the precracks were formed by fatiguing at 100° C, where single-craze crack tip plastic zones could be obtained (see next section). The crack initiation data records the first 0.1 to 0.4 mm of detectable growth. This reflects single-craze extension, which requires a relatively low driving force due to the single-craze nature of the crack tip zone. Thus, a much higher apparent "crack" growth velocity was measured at lower K values than expected. Soon after this initial growth period ended, a multiple-craze crack tip zone formed (at this temperature) and the constant-slope "steady" K–log v line was reached. This behaviour gave the appearance of the higher slope, low K tails in Fig. 3.

In most earlier studies, this tail was not observed and an asymptotic approach to a minimum K was instead reported. This, of course, reflects the initiation process from a starter crack, which was usually inserted by a sharpened razor (see, e.g. [1, 5, 16]). This crack initiation process was obviated in our tests. The important point to note here is that this initial process is not necessarily an intrinsic material property, but is strongly influenced by the crack preparation conditions: the difficulty of initiating and propagating a crack depends on the conditions existing at the initial crack tip. Consequently, the use of the K value at crack initiation as a measure of fracture toughness is suspect.

Once stable crack growth (and a multiple-craze zone) was firmly established, a period of relatively constant $dK/d(\log v)$ was observed. This is referred to as "steady" crack growth, in accord with terminology used by Chan and Williams [16]. Unlike the crack initiation behaviour which is highly dependent on crack preparation techniques, steady crack growth is not, provided that the initial crack is relatively sharp, allowing a "natural" crack to develop. Steady crack

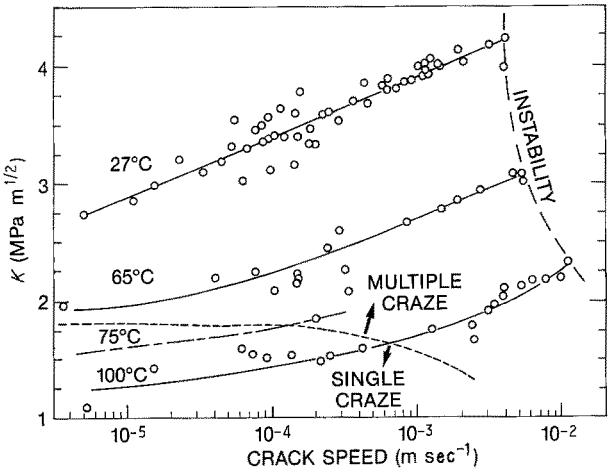

Figure 4 Composite fracture map at four temperatures showing single- and multiple-craze crack tip zones. The transition to unstable crack behaviour is shown by the dashed line.

growth is thus thought to reflect intrinsic material behaviour.

During the steady crack growth period of sample A in Fig. 3, the applied load, the driving force K and the crack velocity attained maximum values, but not all at the same time. These quantities are not, in fact, material constants (for the fracture process), but are instead test dependent values, which depend very strongly on the loading conditions and the sample compliance dependence on crack length. For sample B, the steady crack growth behaviour terminated suddenly in unstable fast fracture. This instability occurred after the load had attained a maximum value and had begun to decrease, although K and the crack velocity were still increasing. Thus, maximum load cannot necessarily be used as a fracture criterion.

Fig. 4 shows a composite fracture map illustrating some of the results obtained for PPO/PS at four different temperatures (over 20 samples were tested at 27° C). In this figure, only the steady crack growth data are plotted and the initiation tails are omitted because they do not represent "equilibrium" data. At about 1 cm sec^{-1}, a transition from stable to unstable crack growth can be observed for the three temperatures. This is denoted by the dashed line labelled "instability" in Fig. 4.

The region of stable crack growth has been further sub-divided into two zones, one where multiple crazing occurs at the crack tip during steady growth and the other where a single craze forms the crack tip plastic zone. This multiple to single-craze transition will be discussed in the next section. The single-craze regime occurs at higher temperatures and slower rates, in accord with Schirrer and Goett's observation [20] in many other amorphous polymers.

The slopes of the K–log v data during steady crack growth indicate the inherent resistance to crack acceleration, with higher values indicating a greater resistance. At 27° C, at velocities between 10^{-4} and 10^{-2} m sec^{-1}, the slope is about 0.50 MPa $m^{1/2}$ per decade of crack speed. In the single-craze zone, on the other hand, at 100° C, at crack speeds between 10^{-5} and 3×10^{-4} m sec^{-1}, the slope drops considerably to 0.10 MPa $m^{1/2}$ per decade of crack speed. This latter value compares with single-craze slope values at room temperature for polystyrene [12] of 0.08 MPa $m^{1/2}$ and PMMA [11] of 0.10 MPa $m^{1/2}$. These smaller values indicate that the single-craze mode is a much easier path for crack propagation. Cracks initiated in this regime have been referred to as "pure cracks" (in polystyrene) by Marshall *et al.* [12].

4.2. Multiple-craze to single-craze transition

Fig. 5 shows optical micrographs of the fracture surface during the multiple-craze and the single-craze growth regions identified in Fig. 4. In all cases, the fracture testing was preceded by fatigue pre-cracking at 100° C in order to produce a sharp single-craze fatigue crack (to be discussed in the next section). In Fig. 5a, crack propagation (in the monotonic loading fracture testing) occurred by a single-craze process. At these high temperatures and low crack speeds, a mirror-like fracture surface was observed. This smooth surface is created by crack propagation within a single-craze plane, with surface roughness reflecting the thickness of collapsed craze fibrils. During fully developed single-craze propagation, the craze/crack growth can lie in the same plane across the entire width of the sample, producing an exceedingly smooth surface. Ironically, this type of fracture surface is usually associated with brittle fast-fracture and not slow steady growth. It does, however, reflect the lower energy for crack propagation observed in brittle fast-fracture.

At higher crack speeds and lower temperatures, a rough fracture surface (whitened) can be observed (Figs 5b, c). This is typical of surface roughening due to multiple crack planes, as well as reflections from sub-surface crazes [24]. The number of crazes that form the crack tip craze bundle can vary depending on the crack speed and temperature, so different degrees of "whitening" can be observed. At the slow steady rates shown in Fig. 4, the whitening is sufficient to make the fracture surface opaque (the PPO/PS blend is normally transparent). However, at very fast rates (in the instability regime, where crack speeds are in excess of 100 m sec^{-1}) the fracture surface, though roughened, is translucent, as the craze density at the propagating crack tip is severely reduced. This is shown in Fig. 5c, where steady crack propagation was followed by a transition to unstable fast fracture. The fracture surface in the unstable region is considerably rougher than that seen in the steady multiple-craze crack growth region, as shown in the electron micrograph of Fig. 6. Concomitantly, the K value during this very fast unstable fracture is reduced from the instability values shown in Fig. 4, this behaviour having been carefully examined by Takahashi and Arakawa [25] for PMMA.

As mentioned earlier, the existence of multiple- and single-craze steady crack growth regimes (Fig. 4) is a generalization of the multiple- to single-craze transition reported for many amorphous polymers at constant crack speeds by Schirrer and Goett [20]. They observed the transition by optical interference measurements of the deformation zones ahead of the propagating crack tips. They also reported a transition in

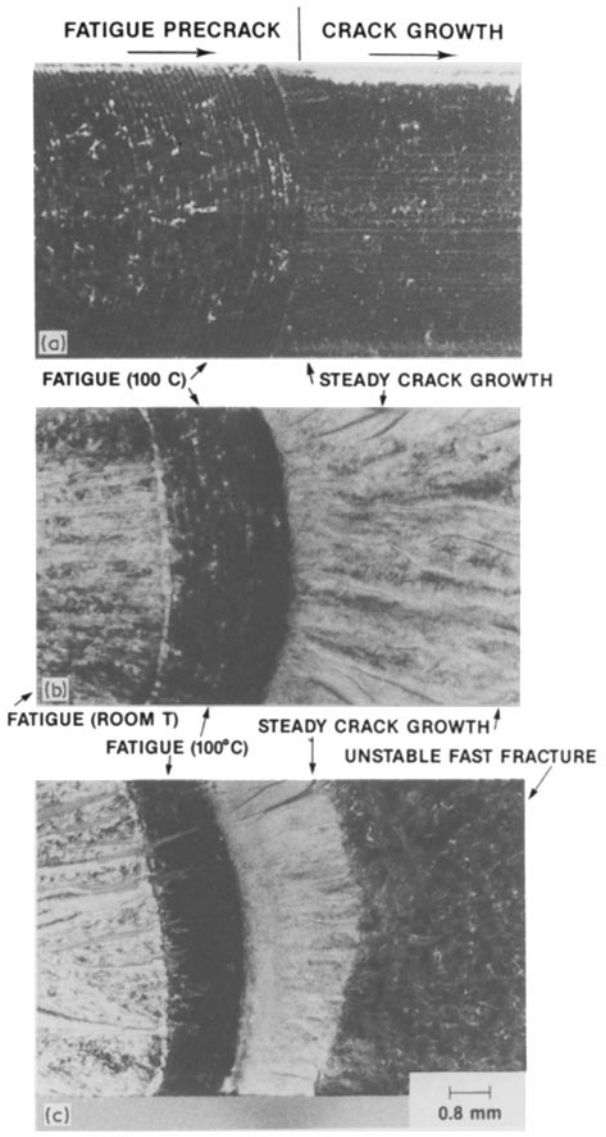

Figure 5 Optical micrographs of the fracture surface showing the steady crack growth single-craze zone (a) and the multiple-craze zone (b, c). The fatigue precrack is indicated by the DCG striations in each photo. Unstable fracture can be seen in (c) after a short distance of steady multiple-craze crack growth.

fracture toughness at the critical temperature and related this transition to the beta mechanical relaxation. They felt that the molecular mechanisms responsible for the beta relaxation led to fibre disentanglement in the craze fibrils at high temperatures, thus encouraging crack growth through the primary craze over the formation of secondary multiple crazes.

4.3. Fatigue

The fatigue analogue of single-craze growth is the discontinuous crack growth (DCG) mechanism. In the DCG mechanism [26–29], a single craze precedes the crack tip and crack growth is arrested for many cycles (up to thousands of cycles are sometimes possible) during which time the crack tip craze breaks down. Sudden crack jumps occur when the craze is sufficiently weakened. These jumps, which are clearly visible to the naked eye, occur along the entire crack front on the same load cycle. The number of cycles between jumps reduces with increasing ΔK. A distinct set of fatigue striation markings (discontinuous growth bands) can be seen on the fracture surface. Fig. 7a

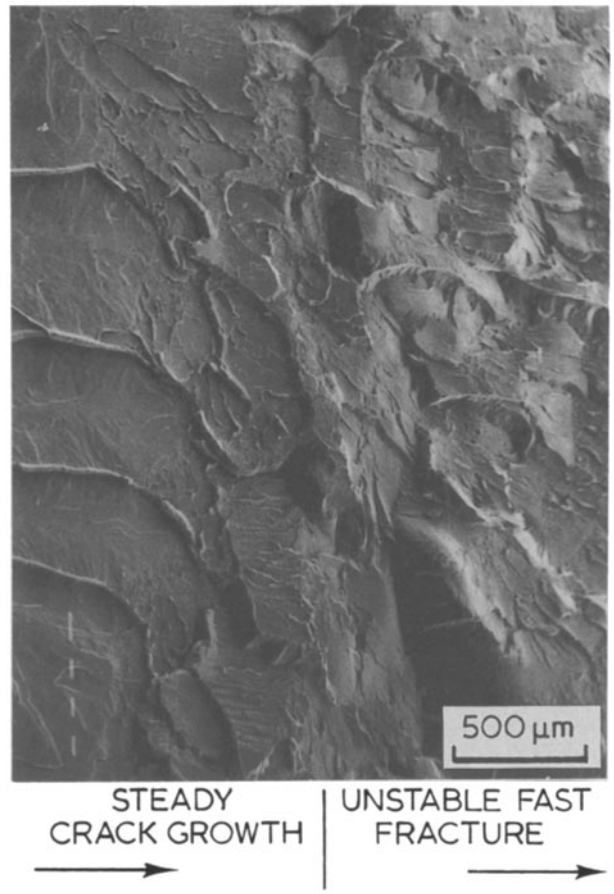

Figure 6 Scanning electron micrograph of the instability transition region from steady crack propagation to unstable fast fracture.

shows these bands for the PPO/PS blend which were formed during the fatigue precracking for the subsequent fracture tests.

The initial fatigue precracking performed at room temperature produced a multiple-craze fatigue crack whose fracture surface showed no clearly visible fatigue striations, but many ridges parallel to the crack growth direction (at very high magnifications, 2 to 3 μm striations could be faintly observed). These ridges were formed by the merger of adjacent craze/crack planes [24]. The secondary precracking was performed at 100° C, under which single-craze crack growth occurred and clearly observable DCG bands could be seen. The multiple plane crack growth transformed into a single crack plane within a few DCG bands (Fig. 7a). DCG bands are usually between 20 and 100 μm [27, 28] and consist of a dark and light band. These alternating dark and light bands are of nearly equal width in PPO/PS. Fig. 7b shows a high magnification micrograph of the light band region, showing surface texture that gives the lightened appearance. The gradation of surface texture from coarse to fine in the direction of crack propagation has been used to model the DCG process as due to the gradual breakdown of the crack tip craze due to fatigue loading [27]. The coarser texture occurs near the crack tip, with the highest stresses and longest load time.

Although the primary and secondary precracking steps were performed in order to prepare as sharp a crack as possible for the subsequent fracture testing, it was realized that the multiple- and single-craze character under fatigue testing was similar to that

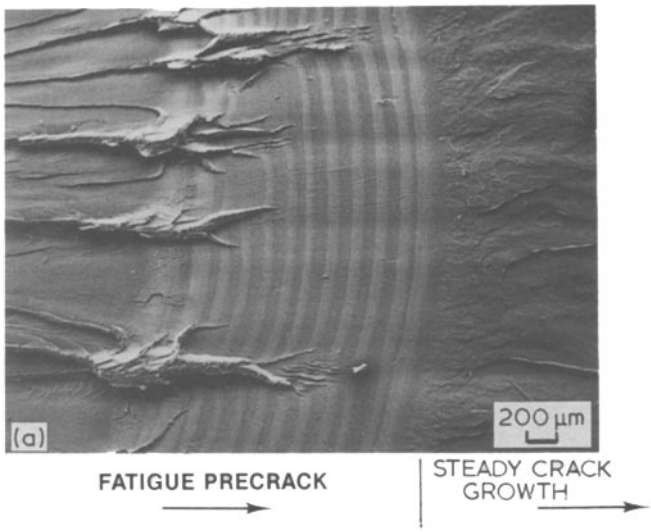

Figure 7 Fatigue discontinuous crack growth (DCG) bands (a) and closeup of the lighter band in the DCG region (b). To the left of the DCG bands is the fracture surface caused by multiple-craze fatigue crack propagation and to the right is slow steady crack growth during the subsequent fracture tests.

observed in steady crack growth. Hence the multiple to single transition under fatigue loading conditions was studied further. Fig. 8 shows two sets of data indicating this transition. Fig. 8a shows the temperature and frequency dependence at a constant driving force, $\Delta K = 0.8\,\mathrm{MPa\,m^{1/2}}$. The multiple-craze mechanism, which produces a whitened fatigue fracture surface (see, e.g., Fig. 5), occupies the lower temperature, slower crack growth region, while the DCG zone occupies the higher temperature, higher crack velocity regime. An intermediate boundary zone can be observed where multiple crazing ends, and single crazing begins, but where distinct DCG bands cannot easily be observed.

The critical temperature for the transition from multiple to single crazing rises with increasing frequency as shown in Fig. 8b. A high activation energy ($\sim 73\,\mathrm{kcal\,mol^{-1}}$) is indicated, which is roughly double the value reported for the beta relaxation in polystyrene [30]. This high value for 50/50 PPO/PS lends

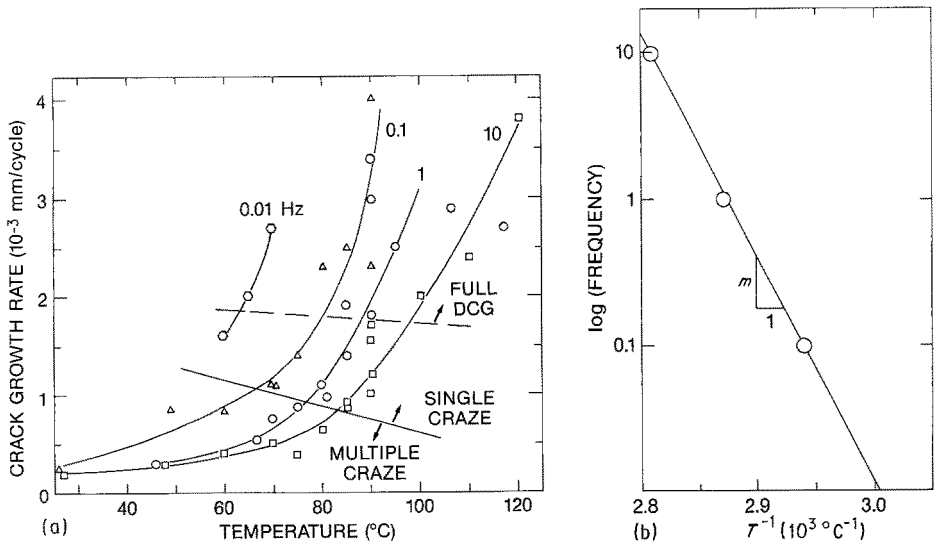

Figure 8 (a) Fatigue map showing the characteristic types of fatigue crack growth behaviour as a function of temperature and frequency: $\Delta K = 0.8\,\mathrm{MPa\,m^{1/2}}$, $R = 0.1$. (b) The activation energy for the transition from multiple to single crazing is determined from the fatigue data of Fig. 8a: $E_A = 2.3Rm = 73\,\mathrm{kcal\,mol^{-1}}$.

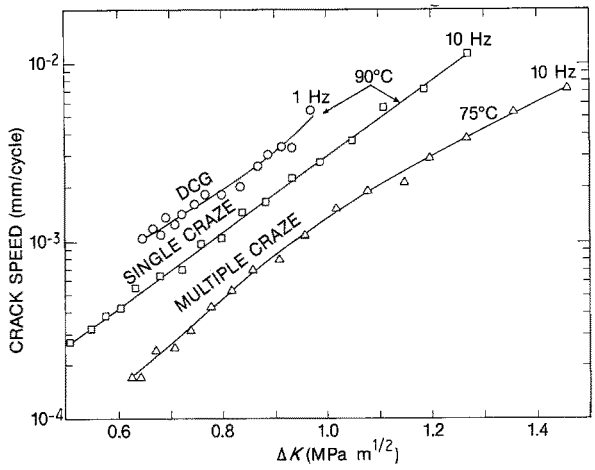

Figure 9 Fatigue crack propagation curves at temperatures and frequencies near the transition zone.

support to the thesis proposed by Schirrer and Goett [20] that movement of relatively large molecular segments (fibre disentanglement) is responsible for the transition to single-craze plastic zones at higher temperatures. Additional work, however, needs to be performed to examine this point much further.

Fig. 9 shows three fatigue crack propagation curves at temperatures and frequencies near the transition zone. At 10 Hz, Fig. 6 shows that the transition occurs between 80 and 85° C for $\Delta K = 0.8\,\mathrm{MPa\,m^{1/2}}$. Thus, data were obtained at 75 and 90° C. At 75° C, multiple crazing was observed throughout the tested range of 0.6 to 1.5 MPa $m^{1/2}$, while at 90° C, single-craze behaviour (but not DCG) was observed from 0.5 to 1.3 MPa $m^{1/2}$. When the frequency was reduced to 1 Hz (at 90° C), however, DCG was then observed throughout the tested range of 0.6 to 1.0 MPa $m^{1/2}$. Each test was performed at constant temperature and frequency, under load control, so ΔK increased with increasing crack length. There was no indication of transitions within a given sample with increasing ΔK, within the range of ΔK tested. Although differences in temperature and frequency must be accounted for, the data do suggest that single-craze fatigue crack growth (and DCG) is an easier mode of crack propagation (requires lower ΔK for comparable crack growth rate). Furthermore, the DCG data show a slightly positive curvature, while the multiple-craze data show a negative curvature.

The fatigue data of Fig. 9 can be crudely compared to the slow crack growth rate data under monotonic loading of Fig. 4, by using K_{max} ($= \Delta K/0.9$) in place of K and $v = f(\mathrm{d}a/\mathrm{d}N)$, where f is the frequency. This is shown in Fig. 10. Large differences can be seen. The slopes of the fatigue data are much steeper than those for the monotonic loading data, which indicates a greater resistance to crack acceleration in fatigue, i.e. a greater increase in crack driving force is required to increase the speed by a given amount. Furthermore, all of the fatigue data presented fall within the single-craze regime of Fig. 4 (for monotonic loading), despite the variety of damage zones found for the fatigue data. The kinetics of crack growth are thus strongly affected by the dynamic nature of the fatigue loading process, when compared to the static nature of monotonic loading.

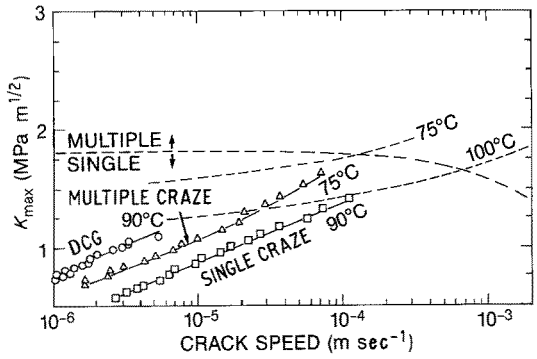

Figure 10 Fatigue results, compared to monotonic loading. The fatigue data are identified by ○, △, □. (– – –) Monotonic loading data at 75 and 100° C. (——) The multiple to single transition curve.

4.4. Strain energy release rate

The strain energy release rate, G, was calculated from Equation 4 using an empirically determined compliance calibration

$$C = \left(\frac{-1}{2.81 + 2.07 \log a(\mathrm{m})}\right)\frac{\mathrm{m}}{\mathrm{MN}} \qquad (18)$$

These values for G were then compared with calculated values for the stress intensity factor, K, using Equation 1. The results from four different samples tested at room temperature are shown in Fig. 11, where K^2 is plotted against G. A linear relationship between K^2 and G is suggested by linear elastic fracture mechanics (Equation 5). Excellent agreement was observed for the room temperature data shown in Fig. 11. The only deviation occurred in the samples tested at the slowest rate of $2.5 \times 10^{-6}\,\mathrm{m\,sec^{-1}}$, well after the load maximum had been reached and the load had reduced to less than 2/3 of the maximum value. At this point the crack had grown more than 1 cm and the crack velocity had also passed through a maximum.

These results indicate that fracture mechanics concepts are quite useful in describing the slow crack growth behaviour of this blend. Either K or G can be

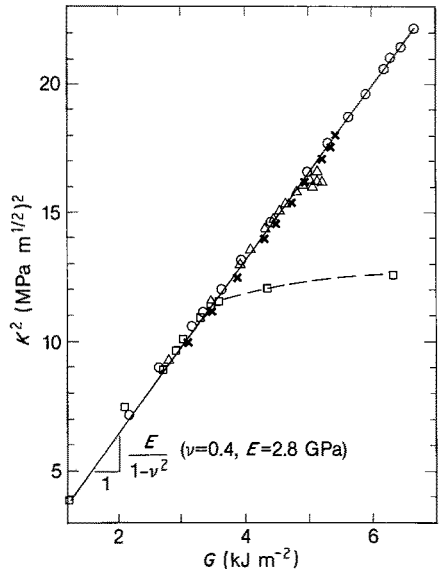

Figure 11 A linear fit is predicted by linear elastic fracture mechanics. K is calculated from Equation 1 and G is calculated from an empirically determined compliance curve (Equations 4 and 18). The results are remarkably good. (○) 2.5×10^{-4}, (×) 2.5×10^{-4}, (△) 5.1×10^{-5}, (□) $2.5 \times 10^{-6}\,\mathrm{m\,sec^{-1}}$.

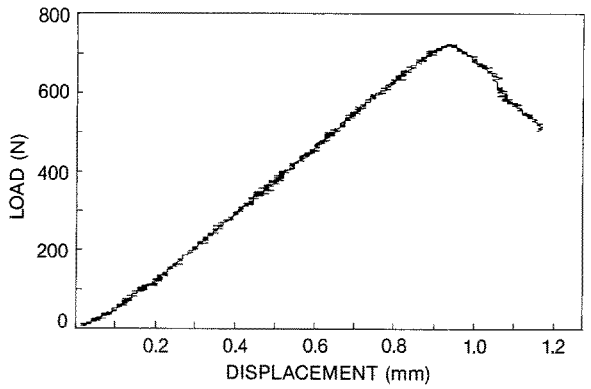

Figure 12 Typical load–displacement curve showing near linearity in the loading curve.

used to describe the instantaneous driving force of the propagating crack, provided instantaneous (current) values of load, crack length and compliance are used.

A further indication of the viability of linear elastic fracture mechanics is the linearity of the load–displacement curve nearly up to the maximum load. Fig. 12 shows a typical example of the loading curve for a sample at room temperature under stroke control.

4.5. Crack velocity

Crack velocities have been calculated for some of the samples using the expression in Equation 7 derived from fracture mechanics principles. In this expression, G is evaluated using the empirical compliance expression (Equation 18), P and D are measured quantities and dP/da is evaluated from measured values of P and a. Fig. 13 shows three such curves (solid lines) compared to the actual measured values of crack velocities. Good agreement can be seen for the three cases presented, again testifying to the usefulness of fracture mechanics concepts.

4.6. Crack instability

The two instability criteria presented in Equations 11 and 17 have been examined for the PPO/PS blend. The

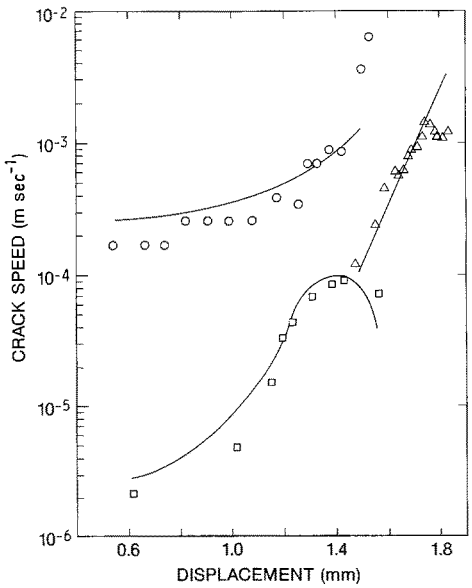

Figure 13 Crack velocities calculated from Equation 7 compared with experimentally determined crack speeds. Crack velocities: (○) 2.5×10^{-4}, (△) 5.1×10^{-5}, (□) 2.5×10^{-6} m sec^{-1}.

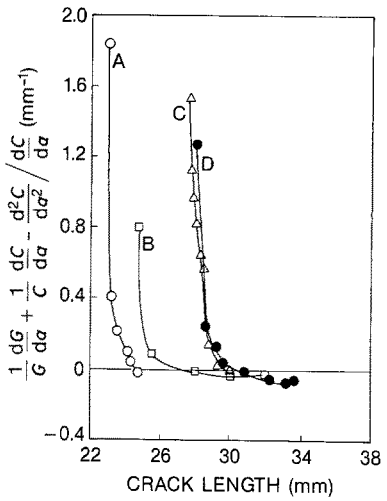

Figure 14 Instability is predicted when the data cross the abscissa ($y = 0$), based on Equation 11.

results are presented graphically in Figs 14 and 15. Four sets of data are shown, with the two at the higher loading rates (A, C) leading to unstable fracture and the two at the lower rates (B, D) leading to completely stable crack growth. In Fig. 14, the left-hand side of Equation 11 is plotted as a function of crack length. When this crosses the abscissa ($y = 0$) then instability is predicted by Equation 11. A similar situation exists for Fig. 15, where the left-hand side of Equation 17 is plotted as a function of crack length and instability is predicted to occur when the data intersect the abscissa. Such a crossing of the abscissa is observed for all four data sets plotted in Fig. 14, but none in Fig. 15, so neither criterion is completely accurate. The stable fracture cases (B, D) did show minima, however, whereas the unstable fracture samples did not. The presence of an instability thus manifests itself in Equations 11 and 17. What is not evident, however, is the ability to predict the onset of the instability from the early crack growth. In both figures, the approach towards the abscissa (during the first millimetre of crack growth) is not indicative of whether unstable or stable crack growth will pursue.

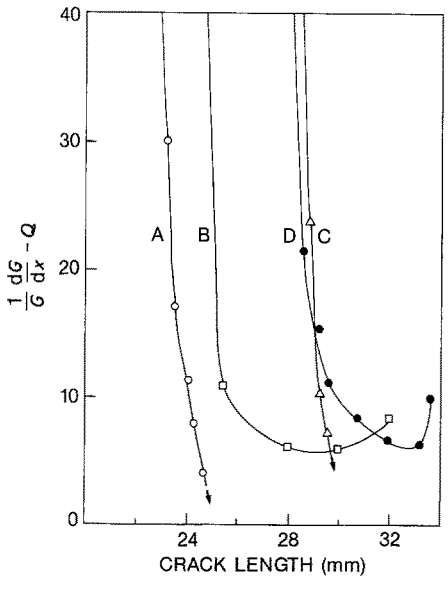

Figure 15 Instability is predicted when the data cross the abscissa, based on Equation 17.

5. Fracture toughness

Based on these observations, we can draw several conclusions about the choice of a meaningful definition of fracture toughness for this class of engineering polymers.

1. The choice of an initiation value is impractical because crack initiation and early crack growth detection is so highly dependent on crack preparation techniques. By preparing fatigue cracks at elevated temperatures and low ΔK, very sharp single-craze cracks were produced for the tests in this study. Initial crack growth was observed at very low K values, producing a "tail" in the K–log v curves. This tail was highly dependent on testing conditions and was therefore treated as anomalous. In studies where sharp razor notches were used, threshold effects were observed because the crack had to initiate from the prepared notch. The initiation event was thus strongly influenced by the preparation technique. Furthermore, the ability to detect the initiation event was highly dependent on the measuring technique and rate of testing, i.e. the slowest detectable crack growth rate was related to the rate at which the testing was performed (e.g. the machine cross-head rate).

2. The choice of a maximum value, such as the load maximum, or the crack velocity maximum, or the stress intensity factor maximum does not necessarily produce an inherent material property. When instability occurs with no or little prior crack growth, these maxima may coincide with a critical material property; however, when significant steady crack growth occurs, the resultant maxima usually do not coincide. This was clearly demonstrated by the examples shown in Fig. 3. The occurrence of the various maxima are clearly a function of intrinsic material properties, testing conditions and the sample geometry (compliance as a function of crack length).

3. There is evidence that fracture instability can be represented by a transition from steady crack growth to unstable fracture, as shown in Figs 1 and 4. This "instability line", as represented on a K–log v plot shows a nearly constant critical crack velocity of roughly 1 cm sec^{-1}, with corresponding critical K values that increase with increasing temperatures. This instability appears to be an inherent material property, corresponding to the limit of steady crack propagation with increasing K. Fracture toughness measures based on this critical instability, however, will be high, non-conservative values.

4. The fracture instability is quite reproducible, provided that steady crack growth has sufficient time to develop. At the crack tip level, this means that the natural crack tip craze zone (be it single-craze or multiple-craze) has evolved into the "equilibrium" behaviour normally observed for those crack growth conditions. Under fast fracture or impact conditions, this is not always the case, and the fracture instability will often occur under non-steady crack growth conditions. Precracks with relatively high initiation thresholds, for example, may not develop equilibrium-like craze zones and can fracture unstably at higher than normal K values (as predicted by fracture maps such as shown in Fig. 4). Excess strain energy released often leads to a large damage zone and subsequent crack bifurcation upon fracture. This phenomenon is quite widely understood and has been the driving force for the requirement for sharp precracks. With sharp initial cracks, on the other hand, instability can sometimes occur "prematurely" at much lower critical K values than otherwise expected. This can generally occur when the loading rate is sufficiently fast that the crack cannot attain equilibrium conditions. In terms of the diagram of Fig. 3, the instability occurs when the crack is still in the initiation "tail" regime of crack growth. Because the location of the tail moves to increasing crack speeds with increasing loading machine displacement rate, by extrapolation, it can be estimated that the tail will intersect the instability line at a machine displacement rate of roughly 0.1 m sec^{-1}. One such test performed at a displacement rate of 0.25 m sec^{-1} led to fracture instability at $K = 3.2$ MPa m$^{1/2}$, which is roughly 25% lower than the critical value expected from Fig. 4. Steady equilibrium crack growth did not precede fracture instability.

In summary, there is no apparently obvious choice for a single measure of fracture toughness. The initiation behaviour, the various maxima and the instability locus are all important facets of the fracture behaviour. Without a complete description, such as the fracture map of Fig. 4, fracture toughness evaluations lose their relevance.

6. Conclusions

This study of the stable crack growth, fracture and fatigue behaviour of a 50/50 miscible blend of PPO/PS has shown the viability of using a linear elastic fracture mechanics description of steady crack propagation which relates the crack velocity to the instantaneous stress intensity factor. This crack growth dependence was strongly influenced by the temperature and the nature of the crack tip craze zone. The rate of steady crack growth increased with increasing temperatures. Furthermore, at higher temperatures and lower crack driving forces, a single-craze crack tip plastic zone was observed, with enhanced crack growth rates. On the other hand, at lower temperatures and high crack driving forces, multiple crazing was observed at the crack tip, and this led to a much greater crack propagation resistance. A fracture instability was observed when the crack speeds reached a critical value, which was roughly 1 cm sec^{-1}. This critical velocity appeared to be insensitive to temperature within the temperature range tested. Several measures of fracture toughness based on crack initiation, maximum load, velocity or K, and fracture instability were examined, with each alternative having both virtues and deficiencies. There is no selection at present which is both an inherent material property and an unequivocal engineering design parameter. For this reason, a complete characterization of the fracture behaviour for polymers, including stable crack growth, instability, impact and fatigue, is necessary and desirable.

References

1. J. G. WILLIAMS, J. C. RADON and C. E. TURNER,

Polym. Engng Sci. **8** (1968) 130.
2. J. G. WILLIAMS, *Int. J. Fract. Mech.* **8** (1972) 393.
3. G. P. MARSHALL, L. H. COUTTS and J. G. WILLIAMS, *J. Mater. Sci.* **9** (1974) 1409.
4. J. C. RADON and N. P. FITZPATRICK, *Engng Mater. Des.* **13** (1970) 1125.
5. F. A. JOHNSON and J. C. RADON, *J. Polym. Sci. Polym. Chem. Edn* **11** (1973) 1995.
6. L. J. BROUTMAN and T. KOBAYASHI, AMMRC CR 71-14, Army Materials and Mechanics Research Centre, Watertown, Massachusetts, 1971.
7. A. G. ATKINS, C. S. LEE and R. M. CADDELL, *J. Mater. Sci.* **10** (1975) 1381.
8. R. D. MARGOLIS, R. W. DUNLAP and H. MARKOVITZ, "Cracks and Fracture", ASTM STP 601, ASTM, 391 (American Society for Testing and Materials, Philadelphia, Pennsylvania, 1976).
9. V. T. TRUONG, P. E. M. ALLEN and D. R. G. WILLIAMS, *Eur. Polym. J.* **22** (1986) 903.
10. J.-C. POLLET and S. J. BURNS, *Int. J. Fract.* **13** (1977) 775.
11. P. TRASSAERT and R. SCHIRRER, *J. Mater. Sci.* **18** (1983) 3004.
12. G. P. MARSHALL, L. E. CULVER and J. G. WILLIAMS, *Int. J. Fract.* **9** (1973) 295.
13. Y. W. MAI, *ibid.* **9** (1973) 349.
14. M. PARVIN and J. G. WILLIAMS, *J. Mater. Sci.* **10** (1975) 1883.
15. P. J. HINE, R. A. DUCKETT and I. M. WARD, *ibid.* **19** (1984) 3796.
16. M. K. V. CHAN and J. G. WILLIAMS, *Polymer* **24** (1983) 234.
17. F. J. McGARRY, J. F. MANDELL and L. H. LEE, *J. Polym. Sci. Polym. Symp.* **72** (1985) 83.
18. E. J. KRAMER and E. W. HART, *Polymer* **25** (1984) 1667.
19. D. MAUGIS, *J. Mater. Sci.* **20** (1985) 3041.
20. R. SCHIRRER and C. GOETT, *ibid.* **16** (1981) 2563.
21. ASTM Test Standard E-399-83, "Standard Test Method for Plane-Strain Fracture Toughness of Metallic Materials", Annual Book of ASTM Standards, Section 2 (American Society for Testing and Materials, Philadelphia, Pennsylvania, 1983) p. 779.
22. C. GURNEY and J. HUNT, *Proc. Roy. Soc. London* **A299** (1967) 508.
23. D. P. CLAUSING, *Int. J. Fract. Mech.* **5** (1969) 211.
24. T. A. MORELLI and M. T. TAKEMORI, *J. Mater. Sci.* **18** (1983) 1836.
25. K. TAKAHASHI and K. ARAKAWA, *Exp. Mech.* **27** (1987) 195.
26. J. P. ELINCK, J. C. BAUWENS and G. HOMES, *Int. J. Fract. Mech.* 7 277 (1971).
27. M. D. SKIBO, R. W. HERTZBERG, J. A. MANSON and S. L. KIM, *J. Mater. Sci.* **12** (1977) 531.
28. M. T. TAKEMORI and D. S. MATSUMOTO, *J. Polym. Sci. Polym. Phys. Edn* **20** (1982) 2027.
29. M. T. TAKEMORI, *Ann. Rev. Mater. Sci. 1984* **14** (1984) 171.
30. N. G. McCRUM, B. E. READ and G. WILLIAMS, "Anelastic and Dielectric Effects in Polymer Solids" (Wiley, London, 1967) p. 414.

Received 7 April
and accepted 5 September 1988